Experimental study of the effect of a slat and vortex generators on the aerodynamic performance of a thick base airfoil

Report's authors: Axelle Viré, Bruce LeBlanc
Scientist in charge of the experiment: Bruce LeBlanc
Technician Engineer: Stefan Bernardy, Emiel Langedijk
Expert support: Nando Timmer, Julia Steiner

1 Methodology

1.1 Experimental setup

The experiment is conducted in the low speed low turbulence tunnel (LTT) of Delft University of Technology[1]. This is an atmospheric tunnel of the closed-throat single-return type, with interchangeable octagonal test sections of size $2.6m \times 1.80m \times 1.25m$ (length×width×height). The maximum Reynolds number for two-dimensional testing is about 3.5 million. Here, the test are performed for $Re = 1.5 \cdot 10^6$ and $Re = 2 \cdot 10^6$. The experimental setup consists of the following components: the main airfoil profile, the slat profile, and the attachment mechanism for testing different slat configurations.

The main airfoil is a DU00-W2-401 profile that is pre-manufactured in composite with a chord length of $c_{\text{main}} = 0.5m$. It was initially fixed to the wind tunnel using tape. However, this led to poor results in the airfoil polars. When a thin silicon seal was used instead, the problem was solved. The slat profile is a custom, cambered airfoil with a chord length equal to $0.3c_{\text{main}}$. The coordinates of the slat element are reported in the appendix (Tab.2). The slat is 3D-printed with an internal structure consisting of stiffening ribs and a main structural steel element. In this study, the streamwise position of the slat trailing-edge is fixed at $s_{\text{slat}} = 0.151c_{\text{main}}$. The effect of two parameters are investigated, as shown in Fig.1: (i) the gap width h_{slat} between the main airfoil and the slat trailing edge, and (ii) the slat angle β_{slat} relative to the main airfoil.

---

[1] https://www.tudelft.nl/en/ae/organisation/departments/aerodynamics-wind-energy-flight-performance-and-propulsion/facilities/low-speed-wind-tunnels/low-turbulence-tunnel/
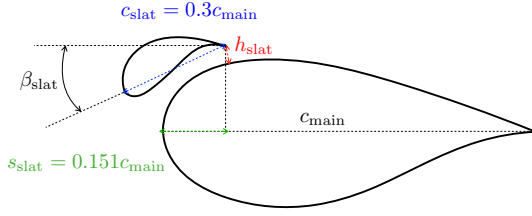
Figure 1: Illustration of the slat parameters of interest in this work: gap width h_{slat} between the main airfoil and the slat, and (ii) the slat angle β_{slat} relative to the main airfoil.
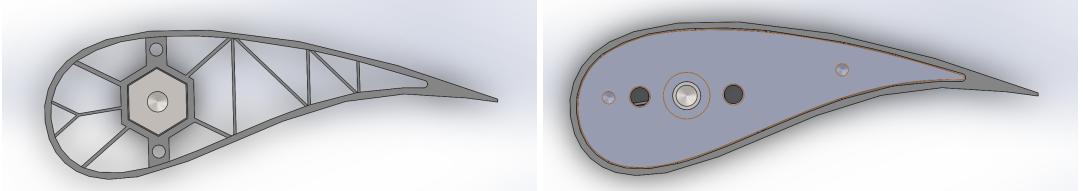

Figure 2: CAD design of the slat cross-section (left) and end plate (right).

In order to vary these parameters, a custom mounting plate is designed and interfaces with the tunnel's machinery for automating airfoil polars. This mounting plate fixes the position of the main airfoil and has a separate set of mounts for the slat. A hexagonal rod is used to support the slat, and has pre-manufactured set points in the mounting plate corresponding to pre-determined values of h_{slat} and β_{slat}. The rod also supports the loads of the slat during high wind speeds. Figure 2 shows CAD views of the cross-section of the slat (left) and the end plate (right).

The set of configurations, and their associated labels, are presented in the test matrix in Tab. 1.

Configuration name	h_{slat}/c_{main}	β_{slat} [^{o}]
A	0.02	16.4
B	0.02	21.4
C	0.02	26.4
D	0.03	16.4
E	0.03	21.4
F	0.03	26.4
G	0.04	16.4
H	0.04	21.4
I	0.04	26.4

Table 1: Set of configurations and associated labels.

In order to reduce three-dimensional effects due to the finite size of the wind tunnel in the spanwise direction, vortex generators (VGs) are installed on the main profile close to the walls, on both the pressure and suction sides of the main airfoil, as shown by Fig. 3 (showing the suction side only). As it will be shown in Section 2, this helps reducing three-dimensional flow

2

Figure 3: Photos of the experimental setup: main profile with slat element (left), main profile with vortex generators (centre), main profile with zig-zag tape (right).
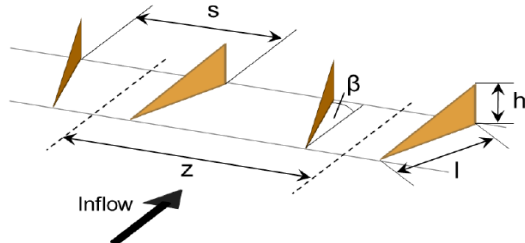

Figure 4: Illustration of the geometrical characteristics of the vortex generators.

effects on the measured pressure distributions. Since vortex generators are commonly used to improve the performances of wind turbine blades, this report also presents results obtained when placing VGs on the main airfoil alone. In that case, the VGs are placed at $x/c_\mathrm{main} = 0.35$. The geometrical characteristics of the VGs are shown in Fig. 4 and the parameter values are as follows: $h/c_\mathrm{main} = 0.01$, $l/h = 2.2$, $z/h = 7.6$, $s/h = 3.2$, and $\beta_\mathrm{slat} = 15.8°$.

1.2 Data acquisition and post-processing

The following measurements are performed. First, 94 and 11 pressure tubes are embedded on the main airfoil and slat profile, respectively. The lift coefficient is obtained by integrating the pressure values on both the main element and the slat. The measured lift coefficient C'_l is expressed as

$$C'_l = \frac{C'_n}{\cos(\alpha)} - C'_d \tan(\alpha), \tag{1}$$

where C'_n is the normal component of the surface integral of the pressure field on the airfoil and α is the angle of attack. The measured lift coefficient is then corrected as [2]

$$C_l = C'_l \left(1 - t_1 - t_2 + t_3 - t_4\right), \tag{2}$$

where

$$t_1 = \frac{\sigma}{\beta^2}, \tag{3}$$

$$t_2 = 5.25 \frac{\sigma^2}{\beta^4}, \tag{4}$$

$$t_3 = \frac{2 - M^2}{\beta^3} \Lambda\sigma \left(1 + \frac{1.1\beta c}{t}\right) \alpha^2, \tag{5}$$

$$t_4 = \frac{(2 - M^2)(1 + 0.4M^2)}{(4\beta^2)} \frac{c}{h} C'_d, \tag{6}$$

and $\sigma = \pi^2/48(c/h)^2$ is the wind tunnel blockage factor, $\beta = \sqrt{1 - M^2}$ is the compressibility factor, M is the measured apparent upstream Mach number, and the body shape factor is set to $\Lambda = 0.9087$. A wake rake equipped with 16 Pitot tubes is further used to measure drag. The measured drag coefficient C'_d is then corrected as

$$C_d = C'_d \left(1 - t_3 - t_4\right). \tag{7}$$

Data are recorded using an electronic data acquisition system and are on line reduced using the HP 9000-712 laboratory computer. A thermal camera enables to visualise the location of flow transition along with the pressure distribution. Wool tufts are also placed on the base airfoil to have a measure of flow separation and identify possible 3D wall effects during testing.

2 Results

2.1 Sensitivity to slat position

Figure 5 shows the lift coefficient C_l as a function of the angle of attack α for different slat configurations and a clean main airfoil. The black dots represent the lift coefficient in the absence of a slat. In that case, the maximum lift coefficient is reached at around $\alpha = 10°$ and remains close to unity. At $\alpha \approx 13°$, the lift coefficient presents a slight increase which is not expected. This feature did consistently appeared for multiple repetitions of the test, even after cleaning the main profile. Therefore, a possible reason for this small disparity could be related to three-dimensional wall effects. As shown in the next subsection, this feature disappears when the Reynolds number increases. For $\alpha > 20°$, the main airfoil enters deep stall and the experimental results should be disregarded. When a slat is added, the disparity around $\alpha \approx 13°$ also disappears and tuft visualisations demonstrate that the flow is rather two-dimensional as expected (Fig. 8). The total maximum lift coefficient is significantly increased (factor up to 2.5) in comparison to the case without slat. For a given gap between the slat and the airfoil, the lift coefficient also increases as the slat angle β_{slat} decreases, except for the smallest gap and angle investigated, i.e.

---

[2]C. Dalton, Allen and Vincenti blockage corrections in a wind tunnel, AIAA Journal 9(9), 1971.
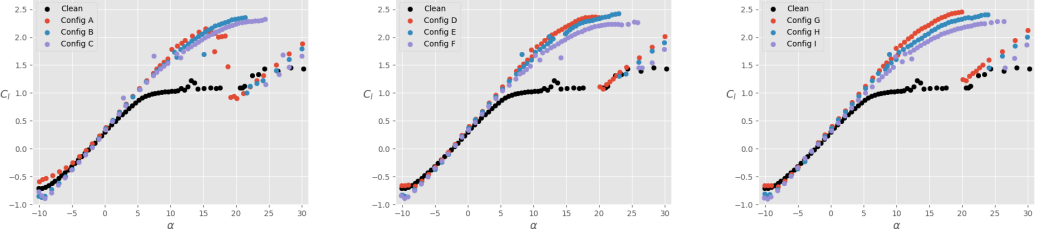
Figure 5: Lift coefficient C_l as a function of the angle of attack α for different slat configurations and a clean main airfoil: $h_{\text{slat}}/c_{main} = 0.02$ (left), $h_{\text{slat}}/c_{main} = 0.03$ (center), $h_{\text{slat}}/c_{main} = 0.04$ (right). The black data are taken without slat, while the coloured data is in the presence of a slat with $\beta_{\text{slat}} = 16.4°$ (red), $\beta_{\text{slat}} = 21.4°$ (blue), $\beta_{\text{slat}} = 26.4°$ (purple). Dots represent the total lift coefficient (main airfoil + slat).
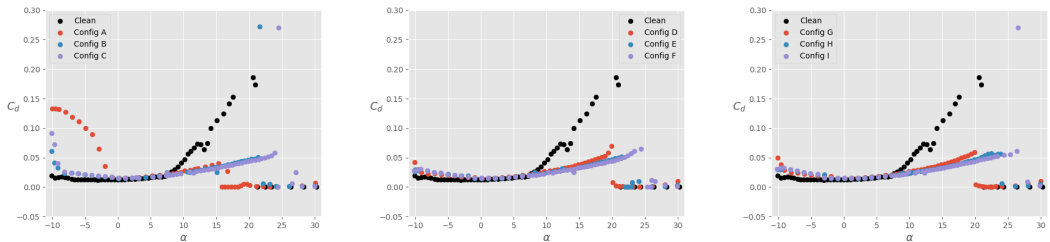

Figure 6: Drag coefficient C_d as a function of the angle of attack α for different slat configurations and a clean main airfoil: $h_{\text{slat}}/c_{main} = 0.02$ (left), $h_{\text{slat}}/c_{main} = 0.03$ (center), $h_{\text{slat}}/c_{main} = 0.04$ (right). The black data are taken without slat, while the coloured data is in the presence of a slat with $\beta_{\text{slat}} = 16.4°$ (red), $\beta_{\text{slat}} = 21.4°$ (blue), $\beta_{\text{slat}} = 26.4°$ (purple). Dots represent the total lift coefficient (main airfoil + slat).

$h_{\text{slat}}/c_{main} = 0.02$ and $\beta_{\text{slat}} = 16.4°$, which stalls already at around $\alpha \approx 15°$. The fact that stall is delayed at increasingly large slat angle is expected due to the increase of effective cambering as β_{slat} increases. Changing the slat gap, for a given slat angle, does not significantly change the lift coefficient. Similarly to Fig. 5, Fig. 6 shows the drag coefficient C_d as a function of the angle of attack. It is apparent that, for all the slat configurations, the total drag coefficient in the range $0° \leq \alpha \leq 7°$ is unaffected by the presence of the slat. For larger angles of attack, the drag coefficient is reduced due to the presence of the slat. Note that, after stall, the values of C_d computed from the wake rake are not reliable. In order to have reliable C_d data during deep stall, drag should be calculated from the pressure distribution and a wake buoyancy correction should be applied. This was not done here.

Figure 9 shows infrared images of the flow past the airfoil at $\alpha = 10°$, without (left) and with (right) slat. Again, it is apparent that the flow is rather two-dimensional in the presence of the slat, whilst some small three-dimensional effects can be seen when the slat is absent. This is probably due to the fact that the slat provides additional mixing, and therefore, may reduce wall effects.

5
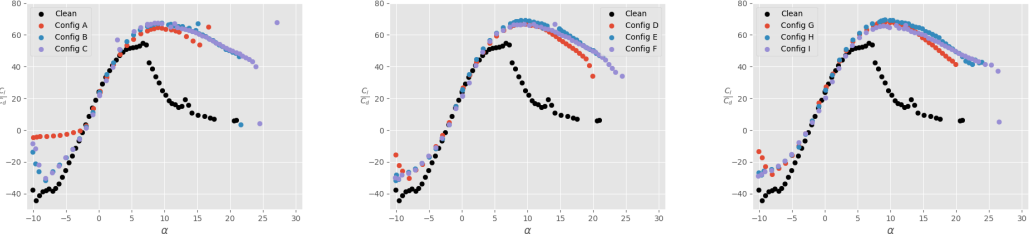
Figure 7: Lift-to-drag ratio C_l/C_d as a function of the angle of attack α for different slat configurations and a clean main airfoil: $h_{\text{slat}}/c_{main} = 0.02$ (left), $h_{\text{slat}}/c_{main} = 0.03$ (center), $h_{\text{slat}}/c_{main} = 0.04$ (right). The black data are taken without slat, while the coloured data is in the presence of a slat with $\beta_{\text{slat}} = 16.4°$ (red), $\beta_{\text{slat}} = 21.4°$ (blue), $\beta_{\text{slat}} = 26.4°$ (purple). Dots represent the total lift coefficient (main airfoil + slat).

Figure 8: Tuft visualisation for a clean airfoil with a slat.

6
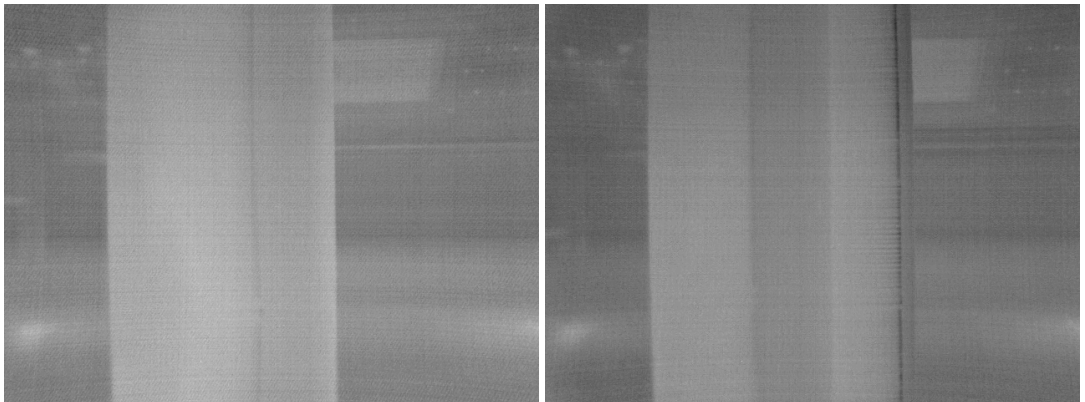
Figure 9: Infrared images of the suction side of the clean main airfoil at an angle of attack $\alpha = 10°$: without slat (left) and with slat under configuration A (right).
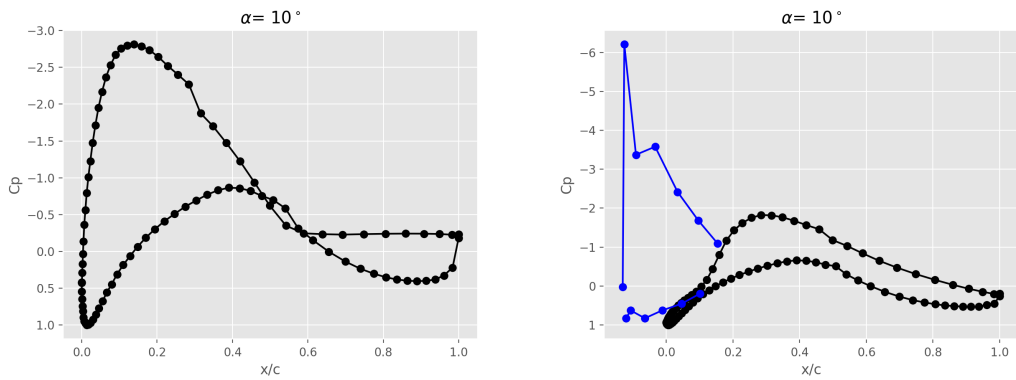
Figure 10: Pressure coefficient C_p at $\alpha = 10°$ for a clean main airfoil: main airfoil alone (left), main airfoil with slat in case A (right), where both the pressure distributions on the main airfoil (black) and slat (blue) are shown.

Finally, the pressure coefficient is shown in Fig. 10 for $\alpha = 10°$. As for the lift and drag values, the pressure distributions were also corrected based on the Allen & Vincenti corrections. It is again clear that the presence of the slat delays flow separation on the main airfoil. It is also apparent that the slat contributes to the main increase in pressure force on the whole system.

2.2 Sensitivity to roughness

In order to assess the sensitivity of the results to surface roughness, the boundary layer on the main airfoil is tripped using a zig-zag turbulator tape placed at the 10% chord location on both the pressure and suction sides. The tape height is calculated based on the Braslow and Knox technique [3], which uses the expected boundary layer thickness at the expected chord location.

---

[3]A.L. Braslow and E.C. Knox, Simplified method for determination of critical height of distributed roughness particles for boundary-layer transition at Mach numbers from 0 to 5, National Advisory Committee For Aeronautics, Technical Note 4363 (1958)

This leads to a tape of dimension $0.2mm$ in height. Furthermore, the tape has a width of $6mm$ and an angle of $30°$. Figure 11 shows the lift coefficient C_l as a function of the angle of attack α for different slat configurations. The black dots again represent the lift coefficient in the absence of slat. As expected, tripping the boundary layer significantly reduces the lift coefficient at low angles of attack. Since the present experimental results are mostly reliable for $\alpha < 20°$, it is difficult to assess whether the zig-zag tape has a significant positive effect at large angles of attack. The negative effect of the zig-zag tape can be alleviated by using vortex generators, as shown in Fig. 12 for the main airfoil without slat. Note that the small abnormality in the lift coefficient at $\alpha \approx 13°$ for the clean case is not observed in the tripped case (with and without VGs). When the slat is mounted on the main airfoil, the zig-zag tape also leads to a loss of C_l at small angles of attack, although this effect is less pronounced than in the absence of slat (Figure 11). Furthermore, similar trends are obtained than with the clean airfoil, namely a decrease in C_l as β_{slat} increases. Also, there is a small decrease of C_l as h_{slat} increases, although this is very small.
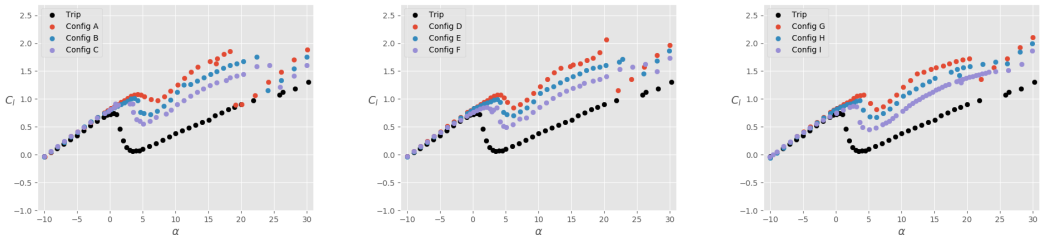
Figure 11: Lift coefficient C_l as a function of the angle of attack α for different slat configurations and a tripped main airfoil: $h_{\text{slat}}/c_{main} = 0.02$ (left), $h_{\text{slat}}/c_{main} = 0.03$ (center), $h_{\text{slat}}/c_{main} = 0.04$ (right). The black data are taken without slat, while the coloured data is in the presence of a slat with $\beta_{\text{slat}} = 16.4°$ (red), $\beta_{\text{slat}} = 21.4°$ (blue), $\beta_{\text{slat}} = 26.4°$ (purple). Dots represent the total lift coefficient (main airfoil + slat).
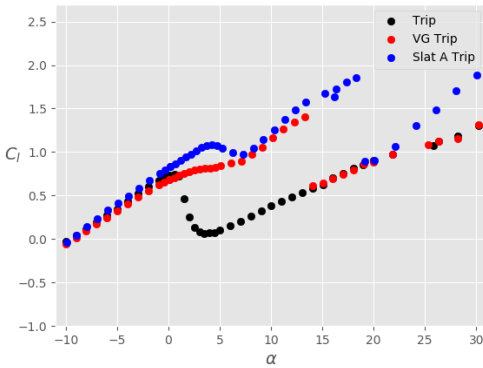
Figure 12: Lift coefficient C_l as a function of the angle of attack α for a tripped main airfoil (without slat): without VGs (red) and with VGs (blue).

8

The drag coefficients are presented in Fig. 13. As expected, drag is larger in the tripped case compared to the clean results. However, the presence of the slat decreases C_d at all positive angles of attack before stall, with the biggest decreases being observed for the smallest slat angles.
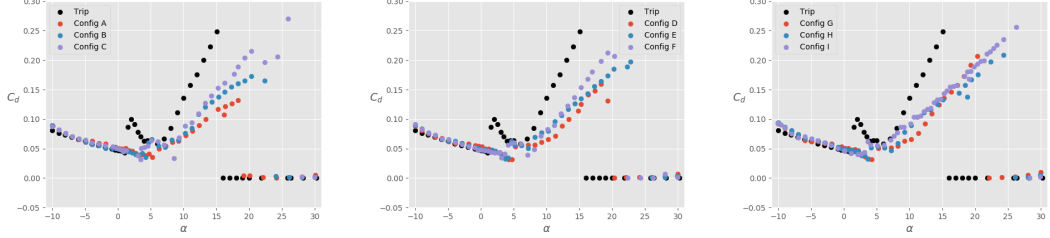

Figure 13: Drag coefficient C_d as a function of the angle of attack α for different slat configurations and a tripped main airfoil: $h_{\mathrm{slat}}/c_{main} = 0.02$ (left), $h_{\mathrm{slat}}/c_{main} = 0.03$ (center), $h_{\mathrm{slat}}/c_{main} = 0.04$ (right). The black data are taken without slat, while the coloured data is in the presence of a slat with $\beta_{\mathrm{slat}} = 16.4°$ (red), $\beta_{\mathrm{slat}} = 21.4°$ (blue), $\beta_{\mathrm{slat}} = 26.4°$ (purple). Dots represent the total lift coefficient (main airfoil + slat).
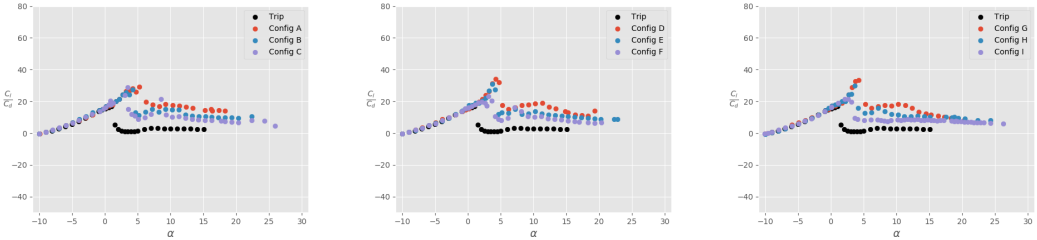
Figure 14: Lift-to-drag ratio C_l/C_d as a function of the angle of attack α for different slat configurations and a tripped main airfoil: $h_{\mathrm{slat}}/c_{main} = 0.02$ (left), $h_{\mathrm{slat}}/c_{main} = 0.03$ (center), $h_{\mathrm{slat}}/c_{main} = 0.04$ (right). The black data are taken without slat, while the coloured data is in the presence of a slat with $\beta_{\mathrm{slat}} = 16.4°$ (red), $\beta_{\mathrm{slat}} = 21.4°$ (blue), $\beta_{\mathrm{slat}} = 26.4°$ (purple). Dots represent the total lift coefficient (main airfoil + slat).

Figure 15 shows infrared images of the flow past the airfoil at $\alpha = 10°$, without (left) and with (right) slat.

Finally, the pressure coefficient shown for $\alpha = 10°$ in Fig. 16.
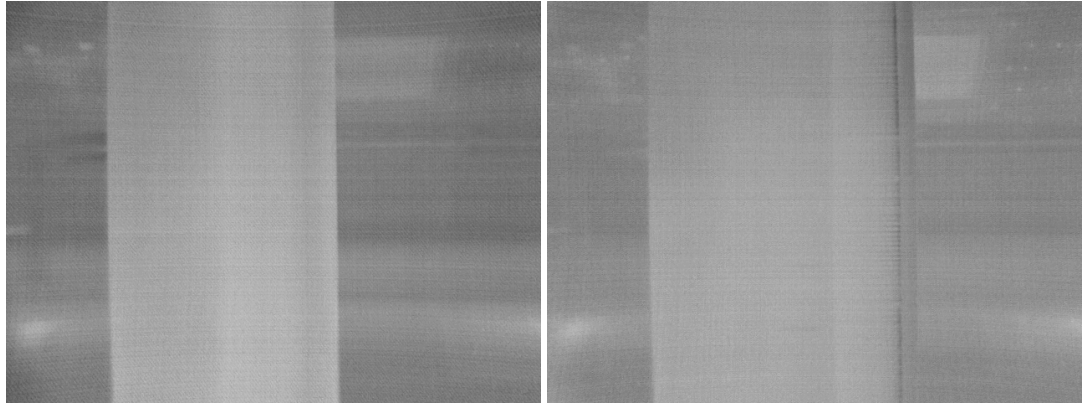
Figure 15: Infrared images of the suction side of the tripped main airfoil at an angle of attack $\alpha = 10°$: without slat (left) and with slat under configuration A (right).
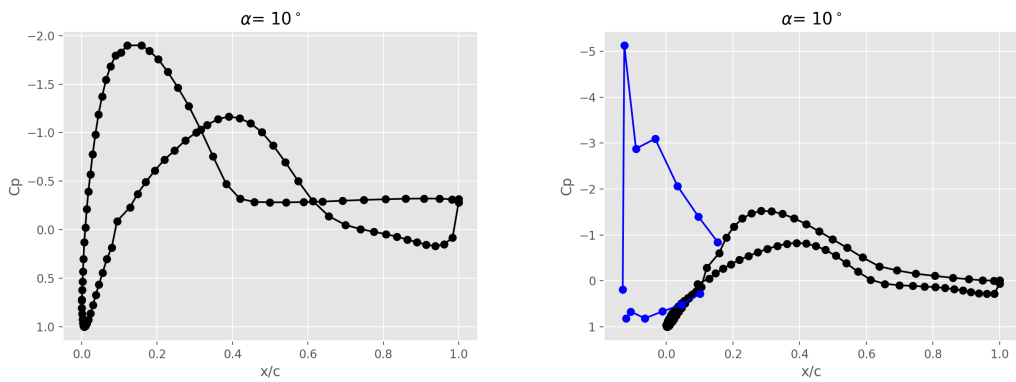
Figure 16: Pressure coefficient C_p at $\alpha = 10°$ for a tripped main airfoil: main airfoil alone (left), main airfoil with slat in case A (right), where both the pressure distributions on the main airfoil (black) and slat (blue) are shown.

2.3 Sensitivity to Reynolds number

Figures 17 and 18 show the polars for the lift and drag coefficients, respectively, without slat and at two different Reynolds numbers. Both clean (left) and tripped (right) conditions are considered. It is apparent that the lift coefficient is rather insensitive to Re in both conditions, at least for the range of Reynolds number investigated here, with only a slightly smaller value of C_l when $Re = 2 \cdot 10^6$. Also, it is worth noting that the disparity observed in C_l at around $\alpha = 13°$ disappears when Re increases. Correspondingly, the drag coefficient is slightly larger when $Re = 2 \cdot 10^6$ and $\alpha \geq 7°$ in the clean conditions. The differences in drag are difficult to assess in the tripped conditions, as the wake rake measurements are not reliable for $3° \leq \alpha \leq 10°$.
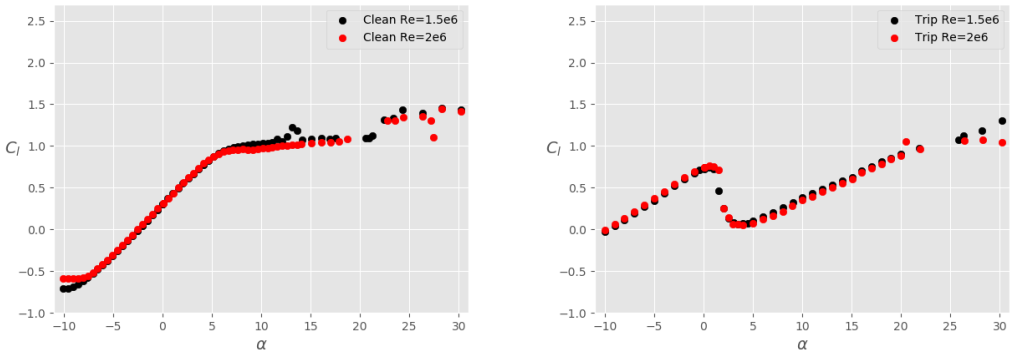
Figure 17: Lift coefficient C_l as a function of the angle of attack α for the main airfoil (without slat) at two Reynolds numbers: $Re = 1.5 \cdot 10^6$ (black) and $Re = 2 \cdot 10^6$ (red). Left: clean airfoil; right: trip airfoil.
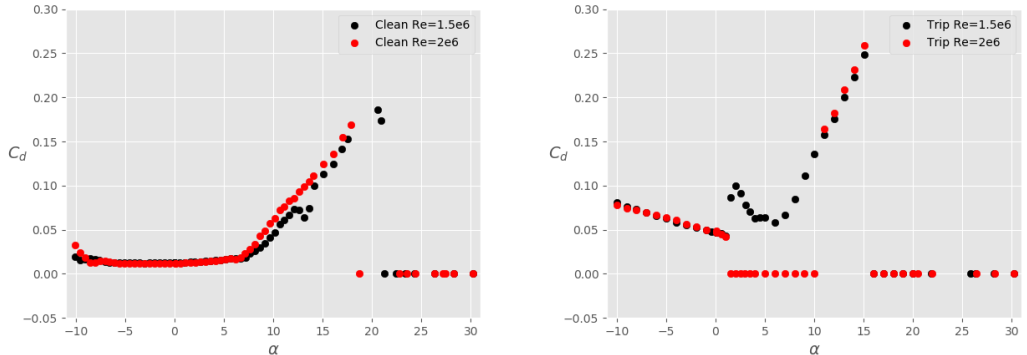
Figure 18: Drag coefficient C_d as a function of the angle of attack α for the main airfoil (without slat): $Re = 1.5 \cdot 10^6$ (black) and $Re = 2 \cdot 10^6$ (red). Left: clean airfoil; right: trip airfoil.

2.4 Comparison of the performances with VGs

Figures 20 and 21 show the polars for the lift and drag coefficients, respectively, without slat but with VGs. Again, both clean (left) and tripped (right) conditions are shown. In both conditions,
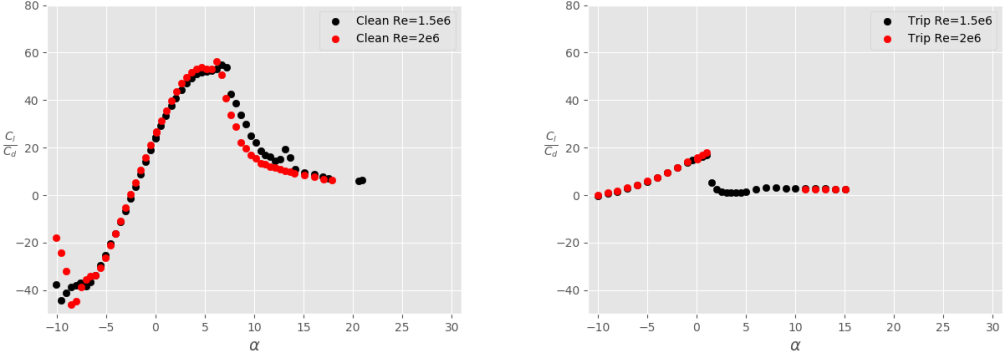
Figure 19: Lift-to-drag ratio C_l/C_d as a function of the angle of attack α for the main airfoil (without slat): $Re = 1.5 \cdot 10^6$ (black) and $Re = 2 \cdot 10^6$ (red). Left: clean airfoil; right: trip airfoil.

it is clear that the lift coefficient is considerably increased due to the presence of the VGs, which delay stall. Comparing these plots to the results obtained with a slat, it is also apparent that the overall lift increase provided by a slat is larger than that provided by the VGs. Of course, the slat brings additional challenges for the structural design of the blade, which are not taken into account here. The total drag coefficient is also slightly smaller with the VGs than it is with the slat.
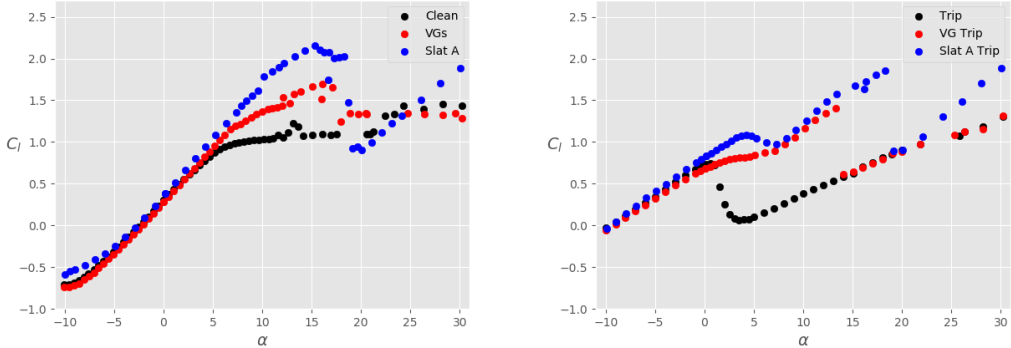
Figure 20: Lift coefficient C_l as a function of the angle of attack α for the main airfoil at $Re = 1.5 \cdot 10^6$, without VGs and without slat (black), with VGs only (red), and with slat only in configuration A (blue). Left: clean airfoil; right: trip airfoil.

Figure 23 shows infrared images of the flow past the airfoil at $\alpha = 10°$ under clean (left) and tripped (right) conditions.

Finally, the pressure coefficient shown for $\alpha = 10°$ in Fig. 24. At this angle of attack, it is clear that the pressure distribution is very similar for both clean and tripped conditions.

12
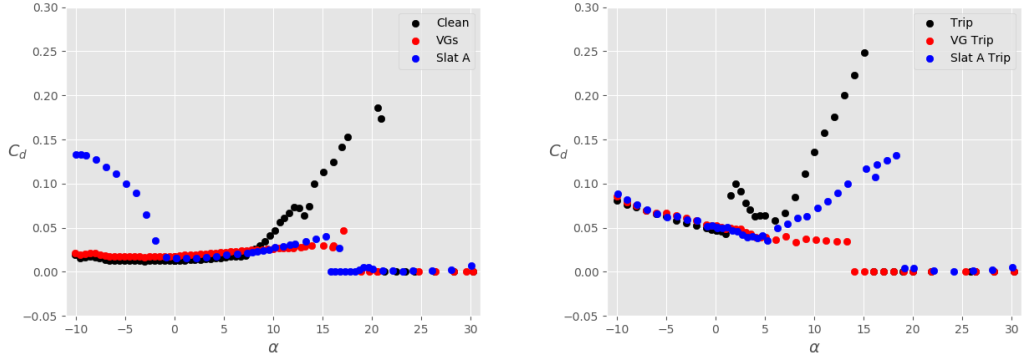
Figure 21: Drag coefficient C_d as a function of the angle of attack α for the main airfoil at $Re = 1.5 \cdot 10^6$, without VGs and without slat (black), with VGs only (red), and with slat only in configuration A (blue). Left: clean airfoil; right: trip airfoil.
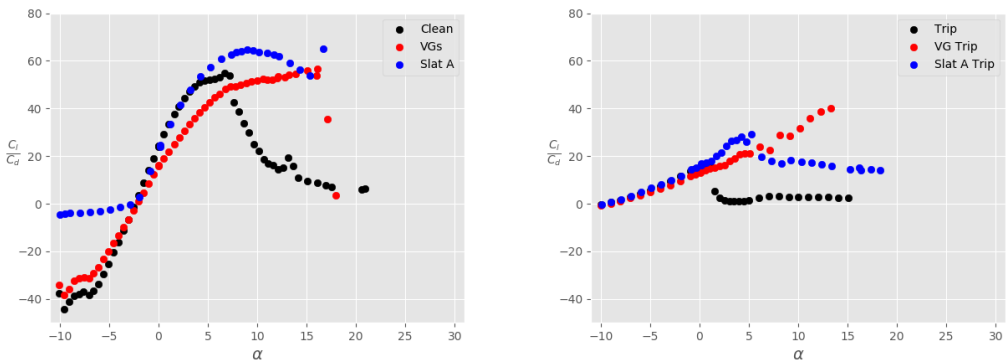
Figure 22: Lift-to-drag ratio C_l/C_d as a function of the angle of attack α for the main airfoil at $Re = 1.5 \cdot 10^6$, without VGs and without slat (black), with VGs only (red), and with slat only in configuration A (blue). Left: clean airfoil; right: trip airfoil.
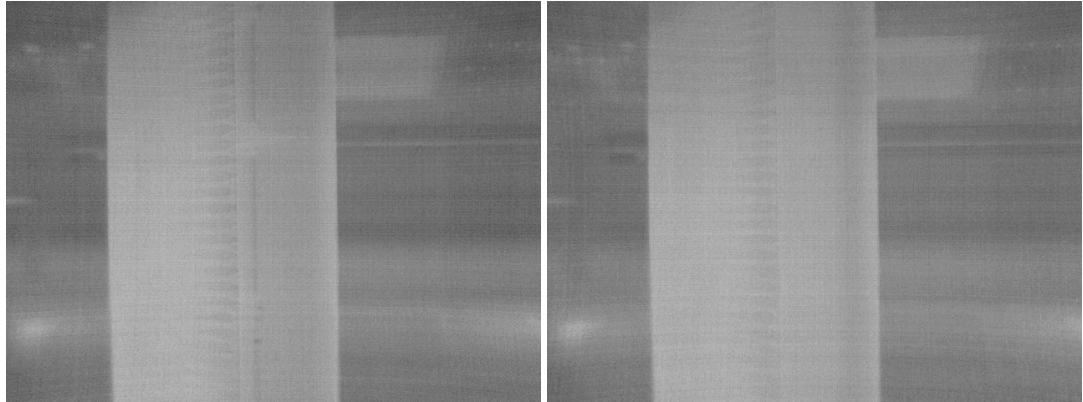
Figure 23: Infrared images of the suction side of the main airfoil with VGs at an angle of attack $\alpha = 10°$: clean (left) and trip (right).
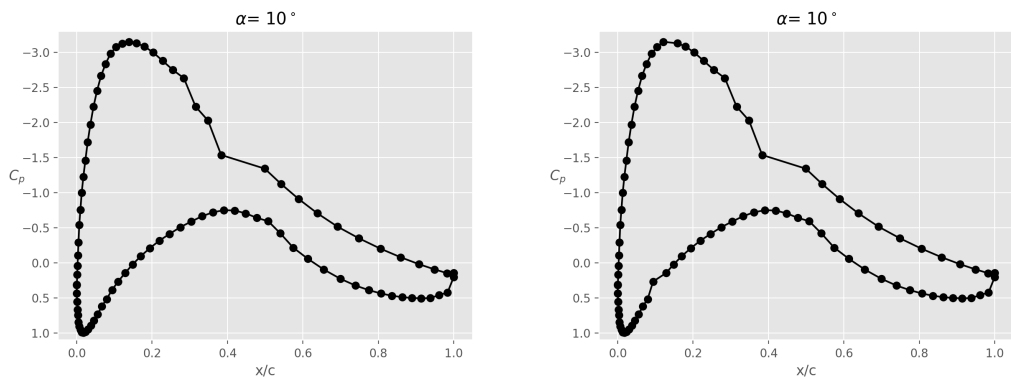
Figure 24: Pressure coefficient C_p at $\alpha = 10°$ for the main airfoil with VGs: clean airfoil (left), trip airfoil (right).

3 Conclusions

This report summarises the main results obtained from the wind tunnel experiments on a DU00-W2-401 airfoil, equipped with a slat or with vortex generators, in both clean and trip conditions. The test results suggest that the use of a slat can significantly increase the aerodynamic performances of the system and delay stall. From a purely aerodynamic point of view, the performances are also better than when vortex generators are used. The results also show some dependencies of the lift coefficient to the position and angular orientation of the slat. In particular, for the range of parameters investigated here, larger slat angles usually lead to smaller C_l. Increasing the distance between the slat and the main airfoil can also lead to slightly better C_l, which suggests that there is an optimal gap between the slat and the airfoil, beyond which the performances will likely decrease again. It is also shown that the use of a slat can partly alleviate the loss of lift at low angles of attack under tripped conditions. This is also the case when using VGs.

Appendix: coordinates of the slat profile

| x-coordinate	y-coordinate
0.000000000000000000e+00	0.000000000000000000e+00
6.411776592915507055e-06	-2.118120231468080192e-03
2.804981566250257916e-05	-4.301167821314075615e-03
6.841992480951066598e-05	-6.546598712740680538e-03
1.308989561228442340e-04	-8.851805659779866942e-03
2.187373519589532096e-04	-1.121412247642543554e-02
3.350616662532271721e-04	-1.363082822439926588e-02
4.828770613633961268e-04	-1.609915133955160810e-02
6.650697804449322162e-04	-1.861627369689532532e-02
8.844095953584786172e-04	-2.117933461427431996e-02
1.143552230109243228e-03	-2.378543479466545957e-02
1.445041759818436891e-03	-2.643164020711499460e-02
1.791312985226702070e-03	-2.911498590630866301e-02
2.184693782729534538e-03	-3.183247979077580975e-02
2.627407429944761223e-03	-3.458110629972774991e-02
3.121574906811939130e-03	-3.735783004852952227e-02
3.669217172223837847e-03	-4.015959940280620921e-02
4.272257416189886164e-03	-4.298334999118298000e-02
4.932523287531629871e-03	-4.582600815665898580e-02
5.651749097110254048e-03	-4.868449434661575176e-02
6.431577996585973421e-03	-5.155572644145870603e-02
7.273564132709571355e-03	-5.443662302189341412e-02
8.179174777145874556e-03	-5.732410657483553995e-02
9.149792431829220293e-03	-6.021510663795458240e-02
1.018671690985104017e-02	-6.310656288285221294e-02
1.129116739187925079e-02	-6.599542813687359066e-02
1.246428445810983214e-02	-6.887867134355364629e-02

1.370713209575031601e-02	-7.175328046169668350e-02
1.502069968203532252e-02	-7.461626530309034555e-02
1.640590394277414293e-02	-7.746466030885347520e-02
1.786359088643014667e-02	-8.029552726441756272e-02
1.939453771373240987e-02	-8.310595795314278111e-02
2.099945470281924798e-02	-8.589307674856766495e-02
2.267898706991372526e-02	-8.865404314529268248e-02
2.443371680553134417e-02	-9.138605422849815918e-02
2.626416448621940111e-02	-9.408634708209567821e-02
2.817079106182871634e-02	-9.675220113551380452e-02
3.015399961831713438e-02	-9.938094044911777170e-02
3.221413711608509672e-02	-1.019699359382629511e-01
3.435149610384337360e-02	-1.045166075359826169e-01
3.656631640801241007e-02	-1.070184262943092435e-01
3.885878679765408794e-02	-1.094729164242301267e-01
4.122904662493531019e-02	-1.118776572742769676e-01
4.367718744112350504e-02	-1.142302852477492109e-01
4.620325458811452846e-02	-1.165284956585716514e-01
4.880724876549186880e-02	-1.187700445257856979e-01
5.148912757311857602e-02	-1.209527503066749193e-01
5.424880702926079823e-02	-1.230744955685242614e-01
5.708616306424334902e-02	-1.251332285990136850e-01
6.000103298963763154e-02	-1.271269649552451697e-01
6.299321694298087859e-02	-1.290537889514043468e-01
6.606247930802804091e-02	-1.309118550850556228e-01
6.920855011053554662e-02	-1.326993894020714049e-01
7.243112638957666105e-02	-1.344146908001954688e-01
7.572987354438941165e-02	-1.360561322712400545e-01
7.910442665675632146e-02	-1.376221620819174374e-01
8.255439178891577079e-02	-1.391113048933044771e-01
8.607934725700600032e-02	-1.405221628189422811e-01
8.967884488004057575e-02	-1.418534164215692062e-01
9.335241120441625795e-02	-1.431038256484879756e-01
9.709954870395279269e-02	-1.442722307055666897e-01
1.009197369554642454e-01	-1.453575528698739516e-01
1.048124337898631020e-01	-1.463587952409478588e-01
1.087770764187958178e-01	-1.472750434306992207e-01
1.128130825368104384e-01	-1.481054661919483095e-01
1.169198513990567789e-01	-1.488493159855959480e-01
1.210967648745176484e-01	-1.495059294864285182e-01
1.253431884747727987e-01	-1.500747280275567530e-01
1.296584723582948073e-01	-1.505552179834887538e-01
1.340419523102764909e-01	-1.509469910918369295e-01

1.384929506979912794e-01	-1.512497247136586342e-01
1.430107774016843580e-01	-1.514631820324313094e-01
1.475947307209965753e-01	-1.515872121916610193e-01
1.522440982569207013e-01	-1.516217503711254633e-01
1.569581577692883423e-01	-1.515668178017505752e-01
1.617361780097908985e-01	-1.514225217191214334e-01
1.665774195305301519e-01	-1.511890552556268141e-01
1.714811354681029520e-01	-1.508666972712381926e-01
1.764465723032165867e-01	-1.504558121229220002e-01
1.814729705958365302e-01	-1.499568493726865792e-01
1.865595656958670134e-01	-1.493703434342628644e-01
1.917055884293617507e-01	-1.486969131584187365e-01
1.969102657602685991e-01	-1.479372613569079065e-01
2.021728214277050129e-01	-1.470921742650521669e-01
2.074924765587658482e-01	-1.461625209429583128e-01
2.128684502568638504e-01	-1.451492526153681795e-01
2.182999601656005484e-01	-1.440534019501437668e-01
2.237862230081707482e-01	-1.428760822753851467e-01
2.293264551022982933e-01	-1.416184867351830967e-01
2.349198728507036482e-01	-1.402818873840059877e-01
2.405656932071045528e-01	-1.388676342197192048e-01
2.462631341177469457e-01	-1.373771541552405440e-01
2.520114149384692359e-01	-1.358119499288280296e-01
2.578097568272986195e-01	-1.341735989530024042e-01
2.636573831125783030e-01	-1.324637521021033160e-01
2.695535196366277697e-01	-1.306841324384799274e-01
2.754973950749349254e-01	-1.288365338773147517e-01
2.814882412308793991e-01	-1.269228197900822419e-01
2.875252933059891380e-01	-1.249449215466409968e-01
2.936077901457275763e-01	-1.229048369959597486e-01
2.997349744608143740e-01	-1.208046288854777578e-01
3.059060930240772302e-01	-1.186464232190989898e-01
3.121203968428349906e-01	-1.164324075538198805e-01
3.183771413068146594e-01	-1.141648292349919658e-01
3.246755863115988738e-01	-1.118459935702177110e-01
3.310149963576052845e-01	-1.094782619418804698e-01
3.373946406246006169e-01	-1.070640498583089739e-01
3.438137930217418092e-01	-1.046058249435746490e-01
3.502717322131540523e-01	-1.021061048659243492e-01
3.567677416190377926e-01	-9.956745520484587553e-02
3.633011093923089185e-01	-9.699248725676799798e-02
3.698711283707719621e-01	-9.438385577939469029e-02
3.764770960048218207e-01	-9.174425667467256407e-02

3.831183142606812697e-01	-8.907642461039294579e-02
3.897940894991692162e-01	-8.638313058042824955e-02
3.965037323299992478e-01	-8.366717940360077210e-02
4.032465574416140841e-01	-8.093140716118762956e-02
4.100218834065467721e-01	-7.817867857305756119e-02
4.168290324623187271e-01	-7.541188431244354173e-02
4.236673302678672370e-01	-7.263393825934809367e-02
4.305361056355044846e-01	-6.984777469258292293e-02
4.374346902384125824e-01	-6.705634542044294766e-02
4.443624182936637967e-01	-6.426261685001376234e-02
4.513186262207791177e-01	-6.146956699511340466e-02
4.583026522758155696e-01	-5.868018242286800190e-02
4.653138361609859830e-01	-5.589745513892114409e-02
4.723515186098131702e-01	-5.312437941127793467e-02
4.794150409478096786e-01	-5.036394853278210182e-02
4.865037446286989420e-01	-4.761915152222781500e-02
4.936169707461597889e-01	-4.489296976410516588e-02
5.007540595211074086e-01	-4.218837358697956341e-02
5.079143497645076666e-01	-3.950831878050543866e-02
5.150971783157168860e-01	-3.685574305107341964e-02
5.223018794563624168e-01	-3.423356241609188527e-02
5.295277842997482276e-01	-3.164466753690257927e-02
5.367742201557945680e-01	-2.909191999032962467e-02
5.440405098715138665e-01	-2.657814847886317763e-02
5.513259711470088753e-01	-2.410614497947664511e-02
5.586299158270148224e-01	-2.167866083107806985e-02
5.659516491679638106e-01	-1.929840276059540533e-02
5.732904690805853409e-01	-1.696802884769562161e-02
5.806456653480418506e-01	-1.469014442813837765e-02
5.880165188195868309e-01	-1.246729793576283052e-02
5.954023005797670631e-01	-1.030197668310900774e-02
6.028022710931473238e-01	-8.196602580673043384e-03
6.102156793245706590e-01	-6.153527794796253766e-03
6.176417618349538952e-01	-4.175030344188286960e-03
6.250797418526059523e-01	-2.263309635084362944e-03
6.325288283200902750e-01	-4.204819350361437827e-04
6.399882149166090661e-01	1.351424214662971367e-03
6.474570790559244227e-01	3.050472647918973934e-03
6.549345808598122654e-01	4.674824284144107715e-03
6.624198621070426229e-01	6.222741899929863651e-03
6.699120451579013702e-01	7.692594962086100538e-03
6.774102318542335466e-01	9.082864522045992761e-03
6.849135023950253531e-01	1.039214817163709725e-02

6.924209141875194984e-01	1.161916506021855484e-02
6.999315006738521250e-01	1.276276097318394288e-02
7.074442701332377403e-01	1.382191347183079136e-02
7.149582044596709540e-01	1.479573709459535216e-02
7.224722579151692248e-01	1.568348861965401797e-02
7.299853558585474023e-01	1.648457238889049908e-02
7.374963934497155149e-01	1.719854569322886925e-02
7.450042343295235625e-01	1.782512421933308763e-02
7.525077092751228935e-01	1.836418755767204453e-02
7.600056148308698134e-01	1.881578477195093926e-02
7.674967119147573236e-01	1.918014002990860167e-02
7.749797244003787666e-01	1.945765829548079182e-02
7.824533376744264856e-01	1.964893108232963065e-02
7.899161971697161722e-01	1.975474226873886671e-02
7.973669068737510024e-01	1.977607397387539170e-02
8.048040278128115732e-01	1.971411249541659902e-02
8.122260765115810743e-01	1.957025430854386627e-02
8.196315234283032547e-01	1.934611212630204385e-02
8.270187913654674094e-01	1.904352102132488012e-02
8.343862538560312681e-01	1.866454460892662606e-02
8.417322335251726795e-01	1.821148129155952117e-02
8.490550004275734253e-01	1.768687056463735113e-02
8.563527703602379360e-01	1.709349938372508801e-02
8.636237031508380291e-01	1.643440859309445654e-02
8.708659009215959923e-01	1.571289941564556897e-02
8.780774063286960196e-01	1.493254000419456766e-02
8.852562007772285524e-01	1.409717205412735000e-02
8.924002026116684139e-01	1.321091747741923693e-02
8.995072652818800751e-01	1.227818513802067524e-02
9.065751754846604893e-01	1.130367764860901181e-02
9.136016512808108336e-01	1.029239822870626000e-02
9.205843401877401577e-01	9.249657624162865160e-03
9.275208172476046009e-01	8.181081088007566282e-03
9.344085830709720764e-01	7.092615422663171854e-03
9.412450618560250781e-01	5.990536083528457886e-03
9.480275993832922854e-01	4.881454343926045977e-03
9.547534609859134047e-01	3.772324521416286526e-03
9.614198294954368063e-01	2.670451265477210429e-03
9.680238031631451801e-01	1.583496906550458608e-03
9.745623935569182050e-01	5.194888664532613769e-04
9.810325234336245703e-01	-5.131728698435605689e-04
9.874310245870453473e-01	-1.505708221071590204e-03
9.937546356713340412e-01	-2.448949415154769247e-03

1.000000000000000000e+00	-3.333333333333333547e-03
1.000000000000000000e+00	3.333333333333333547e-03
9.841773215216269577e-01	9.676253111629761969e-03
9.685476549606405472e-01	1.585529989993487987e-02
9.531094402680488908e-01	2.187324351919246387e-02
9.378611209633556101e-01	2.773281907721970863e-02
9.228011441904609979e-01	3.343672720334397996e-02
9.079279607735674107e-01	3.898763428303879397e-02
8.932400252730807733e-01	4.438172692559985100e-02
8.787357960415161928e-01	4.964094103358178411e-02
8.644137352793986873e-01	5.474850436783341295e-02
8.502723090911691317e-01	5.971339445173457633e-02
8.363099875410864303e-01	6.453810997103205660e-02
8.225252447091314645e-01	6.922511677543578823e-02
8.089165587469100416e-01	7.377684811325492531e-02
7.954824119335558441e-01	7.819570486603436010e-02
7.822212907316352659e-01	8.248405578319034648e-02
7.691316858430503611e-01	8.664423771664701845e-02
7.562120922649413490e-01	9.067855585547242303e-02
7.434610093455910063e-01	9.458928396051474730e-02
7.308769408403273937e-01	9.837866459903857330e-02
7.184583949674282488e-01	1.020489093793607860e-01
7.062038844640234903e-01	1.056021991854869391e-01
6.941119266419988332e-01	1.090406844117472740e-01
6.821810434439004034e-01	1.123664851974330164e-01
6.704097614988354659e-01	1.155816916614326173e-01
6.587966121783785933e-01	1.186883641368675635e-01
6.473401316524736160e-01	1.216885334057288548e-01
6.360388609453380138e-01	1.245842009335130923e-01
6.248913459913654211e-01	1.273773391038585667e-01
6.138961376910287981e-01	1.300698914531815686e-01
6.030517919667852667e-01	1.326637729053123660e-01
5.923568698189786152e-01	1.351608700061315005e-01
5.818099373817424702e-01	1.375630411582058898e-01
5.714095659789049098e-01	1.398721168554249439e-01
5.611543321798895256e-01	1.420898999176370137e-01
5.510428178556220358e-01	1.442181657252850913e-01
5.410736102344311238e-01	1.462586624540432867e-01
5.312453019579531643e-01	1.482131113094529717e-01
5.215564911370353940e-01	1.500832067615587573e-01
5.120057814076386382e-01	1.518706167795449979e-01
5.025917819867418146e-01	1.535769830663715474e-01
4.933131077282451038e-01	1.552039212934102075e-01

4.841683791788724545e-01	1.567530213350807333e-01
4.751562226340768080e-01	1.582258475034871159e-01
4.662752701939409383e-01	1.596239387830538092e-01
4.575241598190835091e-01	1.609488090651614856e-01
4.489015353865608571e-01	1.622019473827837344e-01
4.404060467457712735e-01	1.633848181451228732e-01
4.320363497743579528e-01	1.644988613722461746e-01
4.237911064341119971e-01	1.655454929297222322e-01
4.156689848268770859e-01	1.665261047632567160e-01
4.076686592504518702e-01	1.674420651333290710e-01
3.997888102544938094e-01	1.682947188498280788e-01
3.920281246964224531e-01	1.690853875066885281e-01
3.843852957973232787e-01	1.698153697165271647e-01
3.768590231978499183e-01	1.704859413452788075e-01
3.694480130141292729e-01	1.710983557468325755e-01
3.621509778936637391e-01	1.716538439976680597e-01
3.549666370712349917e-01	1.721536151314914664e-01
3.478937164248077085e-01	1.725988563738718173e-01
3.409309485314321320e-01	1.729907333768770095e-01
3.340770727231485160e-01	1.733303904537101814e-01
3.273308351428899643e-01	1.736189508133455239e-01
3.206909888003859344e-01	1.738575167951648681e-01
3.141562936280660745e-01	1.740471701035935237e-01
3.077255165369625622e-01	1.741889720427366173e-01
3.013974314726148296e-01	1.742839637510151252e-01
2.951708194709723454e-01	1.743331664358022115e-01
2.890444687142981195e-01	1.743375816080591501e-01
2.830171745870720401e-01	1.742981913169717734e-01
2.770877397318942115e-01	1.742159583845863391e-01
2.712549741053889019e-01	1.740918266404459513e-01
2.655176950341074371e-01	1.739267211562265381e-01
2.598747272704318712e-01	1.737215484803731613e-01
2.543249030484784345e-01	1.734771968727359948e-01
2.488670621400005389e-01	1.731945365392067171e-01
2.435000519102927807e-01	1.728744198663544340e-01
2.382227273740941953e-01	1.725176816560619886e-01
2.330339512514915667e-01	1.721251393601622159e-01
2.279325940238228765e-01	1.716975933150738098e-01
2.229175339895806407e-01	1.712358269764377994e-01
2.179876573203154977e-01	1.707406071537534431e-01
2.131418581165397952e-01	1.702126842450146782e-01
2.083790384636305393e-01	1.696527924713459590e-01
2.036981084877333981e-01	1.690616501116386783e-01

1.990979864116653453e-01	1.684399597371872281e-01
1.945775986108189692e-01	1.677884084463251713e-01
1.901358796690653108e-01	1.671076680990614682e-01
1.857717724346575061e-01	1.663983955517163438e-01
1.814842280761343463e-01	1.656612328915579579e-01
1.772722061382230041e-01	1.648968076714381614e-01
1.731346745977435653e-01	1.641057331444287781e-01
1.690706099195115608e-01	1.632886084984578323e-01
1.650789971122418875e-01	1.624460190909455815e-01
1.611588297844518403e-01	1.615785366834408820e-01
1.573091102003649766e-01	1.606867196762571115e-01
1.535288493358140105e-01	1.597711133431083952e-01
1.498170669341449268e-01	1.588322500657460279e-01
1.461727915621197083e-01	1.578706495685942013e-01
1.425950606658202280e-01	1.568868191533865086e-01
1.390829206265515317e-01	1.558812539338019776e-01
1.356354268167452304e-01	1.548544370701013251e-01
1.322516436558627828e-01	1.538068400037627681e-01
1.289306446662994432e-01	1.527389226921187504e-01
1.256715125292870716e-01	1.516511338429917255e-01
1.224733391407977767e-01	1.505439111493301896e-01
1.193352256674477113e-01	1.494176815238455747e-01
1.162562826023997575e-01	1.482728613336472823e-01
1.132356298212676693e-01	1.471098566348799375e-01
1.102723966380191323e-01	1.459290634073588389e-01
1.073657218608791153e-01	1.447308677892062689e-01
1.045147538482336935e-01	1.435156463114881653e-01
1.017186505645329420e-01	1.422837661328493208e-01
9.897657963619480026e-02	1.410355852741505267e-01
9.628771840750838251e-02	1.397714528531040501e-01
9.365125399653712046e-02	1.384917093189100279e-01
9.106638335102272552e-02	1.371966868668929158e-01
8.853231330428804058e-02	1.358867087731370216e-01
8.604826063114093260e-02	1.345620914291232872e-01
8.361345210377749138e-02	1.332231427763651277e-01
8.122712454768532542e-02	1.318701634410444634e-01
7.888852489754739905e-02	1.305034467886484195e-01
7.659691025314500912e-02	1.291232791586048867e-01
7.435154793526152495e-02	1.277299400989189704e-01
7.215171554158569811e-02	1.263237026008093011e-01
6.999670100261495831e-02	1.249048333333436650e-01
6.788580263755918109e-02	1.234735928780759939e-01
6.581832921024374783e-02	1.220302359636816214e-01

22

6.379359998501317464e-02	1.205750117005941896e-01
6.181094478263451930e-02	1.191081638156412936e-01
5.986970403620069797e-02	1.176299308866808890e-01
5.796922884703413492e-02	1.161405465772376161e-01
5.610888104058991271e-02	1.146402398711384440e-01
5.428803322235936646e-02	1.131292353071493700e-01
5.250606883377353928e-02	1.116077532136113826e-01
5.076238220810642965e-02	1.100760099430763556e-01
4.905637862637865498e-02	1.085342181069438444e-01
4.738747437326065737e-02	1.069825868100965083e-01
4.575509679297627696e-02	1.054213218855368367e-01
4.415868434520611729e-02	1.038506261290230714e-01
4.259768666099095213e-02	1.022706995337052671e-01
4.107156459863522957e-02	1.006817395247618652e-01
3.957979029961041645e-02	9.908394119403528266e-02
3.812184724445844691e-02	9.747749753466855571e-02
3.669723030869519870e-02	9.586259967574130292e-02
3.530544581871380289e-02	9.423943711690575820e-02
3.394601160768823817e-02	9.260819796302333096e-02
3.261845707147660589e-02	9.096906915880029199e-02
3.132232322452459944e-02	8.932223672342423648e-02
3.005716275576898397e-02	8.766788598520021403e-02
2.882254008454097904e-02	8.600620181618683080e-02
2.761803141646965165e-02	8.433736886683237954e-02
2.644322479938540638e-02	8.266157180061106668e-02
2.529772017922337496e-02	8.097899552865922557e-02
2.418112945592684748e-02	7.928982544441134928e-02
2.309307653935069315e-02	7.759424765823627612e-02
2.203319740516482619e-02	7.589244923207355553e-02
2.100114015075754681e-02	7.418461841406923107e-02
1.999656505113907301e-02	7.247094487321244227e-02
1.901914461484487118e-02	7.075161993397119375e-02
1.806856363983913583e-02	6.902683681092872114e-02
1.714451926941822080e-02	6.729679084341974593e-02
1.624672104811401147e-02	6.556167973016632788e-02
1.537489097759742532e-02	6.382170376391435584e-02
1.452876357258177549e-02	6.207706606006950422e-02
1.370808591672621583e-02	6.032797282133347400e-02
1.291261771853918772e-02	5.857463351234014348e-02
1.214213136728181479e-02	5.681726155429170526e-02
1.139641198887135498e-02	5.505607252959490716e-02
1.067525750178460395e-02	5.329128842249709896e-02
9.978478672961327983e-03	5.152313385372245258e-02

9.305899173707716035e-03	4.975183831510821691e-02
8.657355635599751909e-03	4.797763600424065356e-02
8.032697706386695766e-03	4.620076605909147205e-02
7.431788105894468477e-03	4.442147279265375170e-02
6.854502681929107097e-03	4.264000592757827279e-02
6.300730466180168299e-03	4.085662083080959794e-02
5.770373730124163034e-03	3.907157874822221599e-02
5.263348040927990322e-03	3.728514703925680379e-02
4.779582317352351964e-03	3.549759941155630066e-02
4.319018885655177657e-03	3.370921615560205920e-02
3.881613535495063560e-03	3.192028437935010010e-02
3.467335575834682229e-03	3.013109824286717281e-02
3.076167890844222486e-03	2.834195919296701727e-02
2.708106995804804989e-03	2.655317619784642105e-02
2.363163093011910829e-03	2.476506598172145690e-02
2.041360127678812711e-03	2.297795325946363001e-02
1.742735843839990969e-03	2.119217097123600457e-02
1.467341840254572562e-03	1.940806051712945166e-02
1.215243626309742099e-03	1.762597199179869595e-02
9.865206779241784442e-04	1.584626441909856021e-02
7.812664934514768067e-04	1.406930598672011604e-02
5.995886495835739622e-04	1.229547428082681734e-02
4.416088572541755413e-04	1.052515652069069621e-02
3.074630175421814732e-04	8.758749793328505021e-03
1.973012775751107240e-04	6.996661288137875911e-03
1.112880864325290170e-04	5.239308531533505391e-03
4.960225104947314502e-05	3.487119621583290811e-03
1.243699211987757060e-05	1.740533462644517585e-03

Table 2: Coordinates of the slat element.

Acknowledgements